Optimizing sampling for surface localization in 3D-scanning microscopy

Marie-Anne Burcklen, Frédéric Galland, Loïc Le Goff

Optimizing sampling for surface localization in 3D-scanning microscopy

Marie-Anne Burcklen[1], **Frédéric Galland**[2,*], **and Loïc Le Goff**[1]

[1]*Aix Marseille Univ, CNRS, Centrale Marseille, Institut Fresnel, Turing Center for Living Systems, Marseille, France.*
[2]*Aix Marseille Univ, CNRS, Centrale Marseille, Institut Fresnel, Marseille, France.*
[*]*Corresponding author: frederic.galland@fresnel.fr*

Compiled November 2, 2022

3D-scanning fluorescence imaging of living tissue is in demand for less phototoxic acquisition process. For the imaging of biological surfaces, adaptive and sparse scanning schemes have been proven to efficiently reduce the light dose by concentrating acquisitions around the surface. In this paper, we focus on optimizing the scanning scheme at constant photon budget, when the problem is to estimate the position of a biological surface whose intensity profile is modeled as a Gaussian shape. We propose an approach based on the Cramér-Rao Bound to optimize the positions and number of scanning points, assuming signal-dependant Gaussian noise. We show that in case of regular sampling, the optimization problem can be reduced to a few parameters, allowing to define quasi-optimal acquisition strategies, first when no prior knowledge on the surface location is available, and then when the user has a prior on this location.

http://dx.doi.org/10.1364/ao.XX.XXXXXX

1. INTRODUCTION

State of the art techniques for 3D-scanning fluorescence microscopy provide high-resolution volumetric images of living tissues. One current limitation lies in the fact that the imaging process is phototoxic and causes photobleaching, as labeled tissues are highly irradiated by excitation light [1]. To reduce photodamage, one solution is to engineer the light dose, either by using pulsed light to avoid the deleterious triplet-state of fluorophores [2], or by using a fast feedback to send just enough light to reach a prescribed signal to noise ratio [3–7]. One can also lower the intensity of excitation light, and couple this reduction with denoising to compensate for the reduced signal [1, 8, 9]. Another solution is to change the setup architecture, such as with the light-sheet microscope that allows to excite only the imaged plane [10]. Eventually, instead of performing a standard plane-by-plane acquisition, one can follow an alternative acquisition scheme, such as axial compressed-sensing [11].

In all of these techniques, the scanning process samples the entire 3D volume. To further reduce the light dose, an idea is to shine light only on points that would provide information of interest. In this regard, an adaptive-scanning fluorescence microscope optimized for the unsupervised imaging of biological surfaces has been designed in [12]. It consists in i) performing a fractional pre-scan of the volume in order to estimate the surface of interest, and then ii) targeting illumination inside a thin shell enclosing this surface. In the case of epithelia – curved cell monolayers –, the pre-scan is performed on a very small fraction ($\sim$ 0.1 %) of the sample space, and therefore contributes very little to the total light dose. Focusing the scan-path exclusively inside the shell allows to dramatically improve the photon budget. A similar strategy is adopted in [13] to estimate the surface of a cell sheet from the two-photon fluorescence emitted in Lissajou pre-scans.

In the aforementioned work, the axial position of the surface is estimated from the set of pre-scanning points. In light of the above, the quality of this estimation is crucial. Indeed, precise estimation allows to restrict the shell as close as possible to the actual structure of interest. But, meanwhile, this estimation must be done with as few photons as possible.

The estimation precision of the surface depends strongly on the sampling strategy adopted during the prescan. In this paper, we search for the sampling scheme that provide the best trade-off between precision and light dose. More precisely, when modeling such surface as a 2D-function S so that $z = S(x, y)$, where (x, y) are the lateral coordinates and z the third coordinate oriented along the sample width, this function $S(x, y)$ can be estimated with scanning intensities along the z-axis for several (x, y)-coordinates, (x_1, y_1), (x_2, y_2), $\ldots$, (x_N, y_N). For the i^{th} coordinates (x_i, y_i), an estimate $\widehat{z}_i$ of the location of the fluorescent epithelium can then be obtained from this scan along z, allowing to recover the function $S(x, y)$ from $(x_i, y_i, \widehat{z}_i)$, $i \in [1, N]$. In this case, it thus becomes fundamental to optimize the acquisition strategy along the z axis. In this work, we will then focus on the following estimation problem: given a couple of coordinates (x, y), our goal is to estimate the

position z_s of the biological surface from several measurements along the z-axis. We assume that we have a fixed photon budget to distribute along z. The question we address is then: for a given (x, y), what are the positions and the number of scanning points along z that provide the most precise estimation of z_s, for a given photon budget? Is it preferable to concentrate this budget on few sampling points along z, with relatively high intensity on each scanning point, or to perform many acquisitions along z with very few photons per acquisition?

Nevertheless, the answer is not trivial, since the problem depends on many parameters, such as the intensity of the fluorescent signal coming from the tissue, the presence of a background signal, the kind of noise and its level in the imaging system, but also on the fact that the user can have – or not – prior knowledge on the surface's location. In this paper, we propose to optimize the sampling strategy using the Cramér-Rao Bound (CRB) that is commonly used to characterize estimation performance [14] and to optimize imaging systems [15–17]. The CRB is a lower bound of the variance of estimation for unbiased estimation algorithms. In our case, the CRB is used to assess for the localization precision. We show that in case of a regular sampling and when the fluorescent signal along z is modeled as a Gaussian shape – which constitutes an accurate approximation in many cases –, we can design optimized sampling strategies that only depend on few reduced parameters. We first study the situation where we have no prior knowledge on the position of the biological surface. We then cover the case where we have a prior knowledge of its approximate position. Such a prior may stem from an iterative procedure to delineate the surface – the precision increasing with each iteration –, or simply from the previous time point in a live imaging context.

The paper is organized as follows. Section 2 describes the model of the noisy fluorescent signal along z, and the general expression of the CRB of the surface's position at fixed photon budget. In Section 3, we analyze the CRB when assuming no prior knowledge on the surface's location, while section 4 tackles the case knowing approximately the surface's location.

2. MODEL AND BOUND ON THE ESTIMATION OF THE AXIAL POSITION OF A BIOLOGICAL SURFACE

A. Model of the fluorescent signal

In this study, we consider a biological surface labeled with fluorescent tags. Typical biological surfaces are epithelium that are layered cell sheets. An example of such an epithelium is shown in Fig 1.a. It consists of a wing imaginal disk of Drosophila melanogaster. The imaginal disk is the precursor, inside the developing larva, of the wing and thorax of the adult fly. It is an important model system to study the regulation of growth and morphogenesis [18]. In Fig. 1.a, the E-cadherin protein involved in the adherens junction between cells is tagged with the green fluorescent protein (GFP) [19]. It is imaged using a conventional confocal spinning-disk microscope coupled with an EM-CCD sensor. A vertical section of the volumetric image is given in Fig. 1.b.

Let us consider the signal s along the z-axis (optical axis) at a given lateral coordinates (x, y). Figure 1.c (red curve) shows a typical profile of this signal s, the maximum corresponding to the location of the adherens junction along z. This signal is sampled over a set of K scanning points $\{z_k; k \in [\![1, K]\!]\}$, and can be modeled as

$$s(z_k) = r(z_k) + n(z_k) \qquad \textbf{(1)}$$

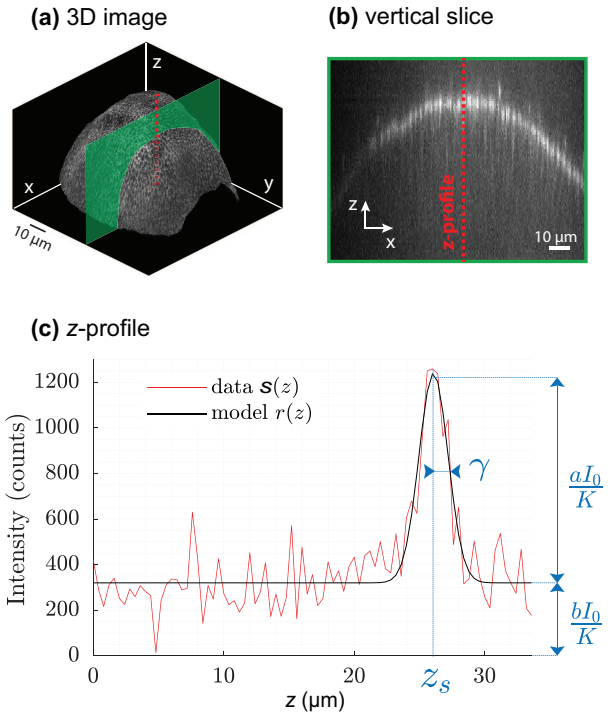

Fig. 1. Example of a fluorescent signal coming from an imaginal disk of Drosophila melanogaster embryo. The cell junctions (E-cadherin) have been tagged with GFP to be fluorescent and lie on a thin sheet. The fluorescent signal is acquired using a spinning-disk confocal microscope coupled with an EM-CCD sensor. (a) 3D image of the imaginal disk. (b) Image corresponding to the green vertical slice shown in (a). (c) z-profil of the signal $s(z)$ (red curve) along the red dotted line shown in (a) and (b), and corresponding gaussian shape model $r(z)$ (black curve). The position of the peak corresponds to that of the cell sheet at the selected (x, y) coordinates. The amplitude of the peak with respect to background is denoted aI_0/K, and the background signal is denoted bI_0/K where I_0 is the total intensity being sent along z axis, and K is the number of scanning samples along z.

where r is a linear combination of a Gaussian shape centered on z_s and of a constant background, as shown in Fig. 1.c (black curve), and $n(z_k)$ denotes the noise corrupting the acquisition. More precisely, r can be written as

$$r(z_k) = \frac{I_0}{K} \cdot \left\{ a \exp\left[-\frac{(z_k - z_s)^2}{2\gamma^2} \right] + b \right\} \qquad \textbf{(2)}$$

where I_0 is the intensity of excitation light to be distributed along z-axis. We assume I_0 is homogeneously distributed so that each point z_k received I_0/K. The parameter γ denotes the standard deviation of the Gaussian shape, and is thus related to the width along z of the adherens junction. The parameter b relates to the proportion of background light reaching the sensor. The parameter a is the amplitude of the Gaussian shape with respect to background. Note that the values of a can strongly vary with respect to (x, y), as for example in Fig. 1.b where only the cell contours contain fluorescent tags. Depending on the kind of cells observed or on the fluorescent tag used, as for example DAPI to tag cell nuclei, the surface on which these cells are distributed may contain larger or smaller non-fluorescent areas, characterized by very low values of the amplitude parameter

a. Although this can affect the difficulty to recover the surface, the optimized scanning strategies proposed in this paper can still be used, provided the modeling of the intensity along z as a Gaussian shape remains valid.

The signal r is corrupted by two sources of noise contained in n: i) electronic noise (mainly thermal and readout noise), which can be modeled as white Gaussian noise of constant variance β, and ii) signal-dependent noise related to photon noise and amplification of the signal. In this work, we consider that, after amplification, the signal we observe contains a sufficient number of counts, so that this signal-dependent noise can be modeled as a Gaussian noise of variance $\alpha r(z_k)$, where α is related to the photoelectron amplification. Thus, the $n(z_k)$ are assumed to be independent Gaussian random variables, with zero-mean and with variance

$$\mathrm{Var}[n(z_k)] = \alpha\, r(z_k) + \beta \tag{3}$$

These parameters α and β allows to cope with various sensor noise models [20–22].

In this paper, the parameters z_s, γ, a, and b are the unknown parameters to estimate – although their values might be known to some extent. In the estimation problem, z_s is the parameter of interest, while γ, a, and b are nuisance parameters. The other parameters constitute experimental parameters.

B. Cramér-Rao bound

Our goal is to estimate z_s the most precisely possible, having a fixed photon budget I_0 to be distributed on the set of scanning points $\{z_k; k \in [\![1, K]\!]\}$. Given this photon budget I_0, what are the number K and the positions z_k that optimize the estimation precision for z_s?

To answer this question, we propose to optimize K and the set of z_k with respect to the Cramér-Rao Bound (CRB) of z_s. The CRB represents the lower bound on the estimation variance that can be obtained with an unbiased estimator. As in [23], but considering the noise model given in Eq. (3), the CRB of z_s can be expressed as (see Appendix A)

$$\mathrm{CRB}_{z_s} = \left[\mathbf{J}^{-1}\right]_{1,1} = \frac{K^2\gamma^2}{I_0^2 a^2}\left[\mathbf{R}^{-1}\right]_{1,1} \tag{4}$$

where $\mathbf{J}$ is the Fisher Information Matrix associated to the estimation of the 4 unknown parameters (z_s, γ, a, b), and where

$$\mathbf{R} = \begin{bmatrix} \Lambda_{2,2} & \Lambda_{3,2} & \Lambda_{1,2} & \Lambda_{1,1} \\ \Lambda_{3,2} & \Lambda_{4,2} & \Lambda_{2,2} & \Lambda_{2,1} \\ \Lambda_{1,2} & \Lambda_{2,2} & \Lambda_{0,2} & \Lambda_{0,1} \\ \Lambda_{1,1} & \Lambda_{2,1} & \Lambda_{0,1} & \Lambda_{0,0} \end{bmatrix} \tag{5}$$

with

$$\Lambda_{p,q} = \sum_{k=1}^{K} \frac{(Z_k - Z_s)^p\, e^{-\frac{q(Z_k-Z_s)^2}{2}}}{\frac{\alpha I_0}{K}\left[a e^{\frac{-(Z_k-Z_s)^2}{2}} + b\right] + \beta} \tag{6}$$

with defining the reduced parameters $Z_s = z_s/\gamma$, and $Z_k = z_k/\gamma$.

This expression depends on z_s, which is the parameter of interest, and on the parameters a, b and γ, which are generally unknown. Note that, usually, an approximate value of γ is known, as it corresponds to the measurable thickness of the cell sheet. The expression also depends on the intensity I_0, on the noise parameters α and β, and on the number K and the positions z_k ($k \in [\![1, K]\!]$) of the scanning points. Our goal is to analyze how to optimize K and z_k to decrease CRB_{z_s}.

In the following, we will focus on regular sampling strategies, i.e. so that the sampling step $z_{k+1} - z_k$ is constant, because such strategies can easily be implemented experimentally and because their optimal settings are tractable computationally. Moreover, two situations will be considered: first, when we have no a priori knowledge on the surface's location z_s (section 3), and second, when we know approximately in which interval z_s has to be searched (section 4).

3. OPTIMAL SAMPLING WITHOUT PRIOR ON THE SURFACE LOCATION

In this section, we assume that we have no prior information on the position z_s of the biological surface. In this case, the whole axial range available has to be scanned, with scanning points z_k uniformly distributed along z. Our goal is then to find the optimal value of the sampling step, *i.e.* the spacing between two consecutive scanning points.

A. Reformulation of the optimization problem

Let us denote $[z_{\min}, z_{\max}]$ the axial range available. As previously mentioned, the scanning points z_k will be uniformly distributed on $[z_{\min}, z_{\max}]$ so that $z_{k+1} - z_k = \delta$, with δ denoting the constant sampling step, and $z_1 = z_{\min} + \delta/2$ and $z_K = z_{\max} - \delta/2$. Let us define $l = z_{\max} - z_{\min}$ the length of the interval to probe. The number K of scanning points is then $K = l/\delta$. Thus, optimizing the scanning strategy is equivalent to determine the value of δ that minimizes CRB_{z_s}.

Let us define the reduced parameters $\Delta = \delta/\gamma$ and $L = l/\gamma$. The coefficients $\Lambda_{p,q}$ of Eq. (6) can be rewritten as

$$\Lambda_{p,q} = \frac{1}{\alpha I_0 b/L + \beta}\,\widetilde{\Lambda}_{p,q} \tag{7}$$

where

$$\widetilde{\Lambda}_{p,q} = \sum_{k=1}^{L/\Delta} \frac{(Z_k - Z_s)^p\, e^{-\frac{q}{2}(Z_k-Z_s)^2}}{\lambda\left[1 + \eta e^{-\frac{(Z_k-Z_s)^2}{2}}\right]\Delta + (1-\lambda)} \tag{8}$$

with

$$\eta = \frac{a}{b} \text{ and } \lambda = \frac{\alpha I_0 b/L}{\alpha I_0 b/L + \beta} \tag{9}$$

The parameter η is the signal to background ratio. The parameter λ is a noise coefficient that takes values between 0 and 1. In the expression of λ, the quantity $\alpha I_0 b/L$ corresponds to the variance of the signal-dependent noise that comes from the background, on a typical length of γ, and β is the variance of the electronic noise. Therefore λ can be seen as the proportion of signal-dependent noise with respect to the total amount of noise, considering the background only. When $\lambda \to 0$, $\beta \gg \alpha I_0 b/L$, which means that the electronic noise becomes predominant, whereas, when $\lambda \to 1$, the signal-dependent noise is predominant. It corresponds to the case of an ideal sensor without additive electronic noise. Note that when $\lambda = 1$, the CRB of z_s corresponds to that obtained in Poisson noise regime.

In the following, we define the matrix $\widetilde{\mathbf{R}}$ that is of the same form of matrix $\mathbf{R}$ given in Eq. (5), but filled with the $\widetilde{\Lambda}_{p,q}$ coefficients instead of $\Lambda_{p,q}$. The CRB of z_s becomes

$$\mathrm{CRB}_{z_s} = \frac{L^2\gamma^2\,(\alpha I_0 b/L + \beta)}{I_0^2 a^2}\,\frac{[\widetilde{\mathbf{R}}_1^{-1}]_{1,1}}{\Delta^2} \tag{10}$$

Finding the value of δ that minimizes CRB_{z_s} is thus equivalent to find the value of $\Delta = \delta/\gamma$ that minimizes $[\widetilde{\mathbf{R}}^{-1}]_{1,1}/\Delta^2$.

From Eq. (8), it comes that $[\widetilde{\mathbf{R}}^{-1}]_{1,1}$ is a function of Z_s, η, λ, and of the set $\{Z_k\}_{k=1,\dots,K}$ *i.e.* of the set $\{Z_1, L, \Delta\}$. We can check that $[\widetilde{\mathbf{R}}^{-1}]_{1,1}$ depends no more on L, as soon as L is sufficiently high (typically $L = l/\gamma \gtrsim 10$). Indeed, increasing L while keeping all other parameters constant only improves the estimation of the unknown background parameter b, and has no impact on the estimation precision of a, γ and z_s.

Because $[\widetilde{\mathbf{R}}^{-1}]_{1,1}$ depends on Z_s itself, which is to estimate, we propose to follow a minimax approach. We minimize the maximal CRB – the worst CRB value – over all Z_s values. When ignoring bounding effects obtained when z_s is close to $z_{\min}$ or $z_{\max}$ (within a typical distance of 3γ), it comes that CRB_{z_s} varies as a Δ-periodic function of Z_s. We thus only have to consider the maximal value of CRB_{z_s} over all Z_s in $[Z_0 - \Delta/2, Z_0 + \Delta/2]$ with $Z_0 = (Z_{\max} + Z_{\min})/2$. We then search for the optimal Δ value

$$\Delta_{opt} = \underset{\Delta}{\operatorname{argmin}} \widetilde{\mathrm{CRB}}_{z_s} \tag{11}$$

with

$$\widetilde{\mathrm{CRB}}_{z_s} = \max_{Z_s \in [Z_0-\Delta/2, Z_0+\Delta/2]} \frac{1}{\Delta^2}[\widetilde{\mathbf{R}}^{-1}]_{1,1} \tag{12}$$

Now, provided L is sufficiently high, and ignoring Z_s-bounding effects, Δ_{opt} depends only on λ and η. Through these two reduced parameters λ and η, Δ_{opt} takes into account the parameters of the acquisition and of the model (*i.e.* $z_{\min}$, $z_{\max}$, I_0, a, b, γ, z_s, α and β).

B. Analysis

Figure 2.a shows the evolution of $\widetilde{\mathrm{CRB}}_{z_s}$ with respect to Δ, when $\eta = 1$ and for several values of λ. Note that when $\lambda = 0$, $\widetilde{\mathrm{CRB}}_{z_s}$ no more depends on η (see Eq. (8)). For ease of comparison between different λ values, the CRB has been divided by its minimal value $\min_\Delta \widetilde{\mathrm{CRB}}_{z_s}$.

As can be seen in Fig. 2.a, for all conditions, $\widetilde{\mathrm{CRB}}_{z_s}$ presents a clear minimum, and increases to infinity at large Δ. A contrario, when $\Delta \to 0$, the behavior of $\widetilde{\mathrm{CRB}}_{z_s}$ depends on λ. When $\lambda = 1$, CRB_{z_s} stays almost constant and close to its minimal value, as long as $\Delta < 1.3$ (red curve in Fig. 2.a). When $\lambda < 1$, $\widetilde{\mathrm{CRB}}_{z_s} \to \infty$ when $\Delta \to 0$. Indeed, $\lambda < 1$ corresponds to $\beta > 0$, the case of a non-ideal sensor. In this case, when $\Delta \to 0$, the number of scanning points increases. Then, because the photon budget is fixed, the number of photons per scanning points tends to zero while the variance β of the electronic noise remains constant.

From the position Δ_{opt} of this minimum, for each λ and η, we can derive the optimal sampling step $\delta_{opt} = \gamma\, \Delta_{opt}$, provided γ is known. Fortunately, in many biological configurations an approximate value of γ is generally known, allowing then to derive an approximate value of δ_{opt}. Considering this point, our goal is then not necessarily to determine the precise value Δ_{opt}, but more interestingly to determine a range of Δ-values, for which the performance are close to the optimal CRB value.

Accordingly, Figure 2.b shows the range of Δ, for which the increase in $\widetilde{\mathrm{CRB}}_{z_s}$ from its minimal value is bounded to 20 %, as a function of λ. It has been plotted for several values of η varying from 0 to 10. Note that although $\eta = 0$ corresponds to a situation for which it is not possible to estimate z_s (since $a = 0$), it has been plotted as the limit case of null signal-to-background ratio. The larger the area where the increase in CRB is lower than 20 %, the more robust to an uncertainty on the parameter γ.

Having an approximate value $\tilde{\gamma}$ of γ, we can set the value of the spacing δ so that $\Delta = \delta/\tilde{\gamma}$ corresponds to the middle of the Δ-range (see dashed lines in Fig. 2.b). Furthermore, although the signal-to-background ratio $\eta = a/b$ is another unknown that can strongly varies in the image, it can be seen that the middle of this Δ-range is almost independent of η, even when η is varying from 0 to 10. Furthermore, it can be noted that setting for example $\Delta = 1.3$ is a robust solution, whatever the value of λ.

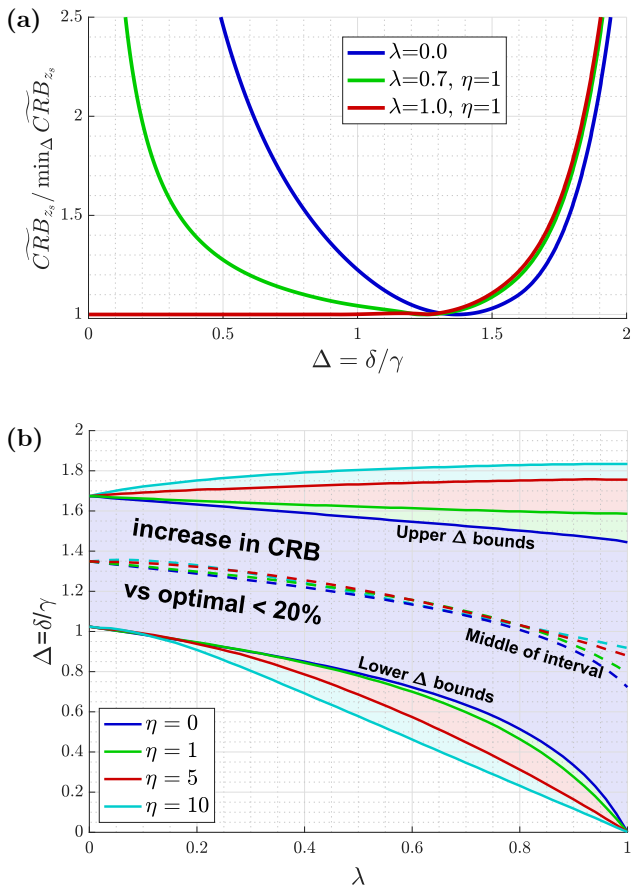

Fig. 2. (a) Evolution of $\widetilde{\mathrm{CRB}}_{z_s}$ / $\min_\Delta \widetilde{\mathrm{CRB}}_{z_s}$ as a function of $\Delta = \delta/\gamma$ and for several values of λ and η. (b) Evolution as a function of λ (and for several values of η) of the range of Δ-values for which the increase in $\widetilde{\mathrm{CRB}}_{z_s}$ with respect to the optimal value $\min_\Delta \widetilde{\mathrm{CRB}}_{z_s}$ is lower than 20 %. Plain curves correspond to the upper and lower bounds of the Δ ranges and dashed curves to the middle of the Δ-ranges.

Let us now analyze the robustness of this approach to an error on γ. We denote γ the true standard deviation of the Gaussian, and $\widetilde{\gamma} = \gamma(1 \pm \epsilon)$ the erroneous value used to define the scanning scheme. With these notations, the reduced parameter $\Delta = \delta/\gamma$ is changed into $\widetilde{\Delta} = \delta/(\gamma(1 \pm \epsilon)) \approx \Delta(1 \pm \epsilon)$. This means that Δ has the same relative error ϵ as γ. Figure 3 shows how an error on γ affects the estimation of z_s depending on noise parameters. To do so, we first set Δ near its optimal value, *i.e.* in the middle of the Δ-range aforementioned (where the increase in CRB with respect to optimal is lower than 20% - see

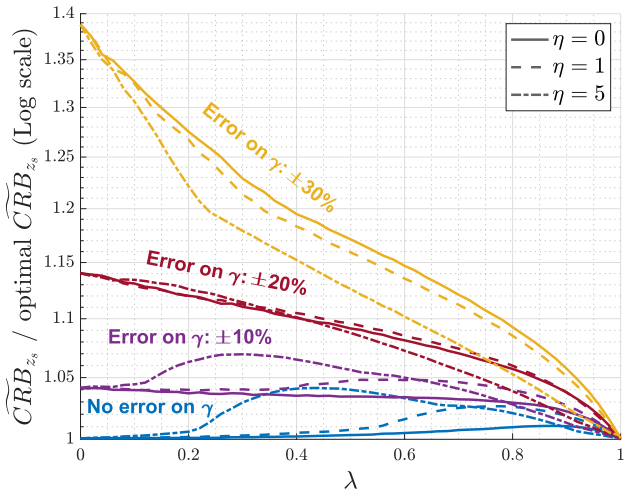

Fig. 3. Robustness to an error on γ. Evolution of $\widetilde{\text{CRB}}_{z_s} / \min_\Delta \widetilde{\text{CRB}}_{z_s}$ as a function of λ in the ideal case where γ is perfectly known (in blue) and in case of an error on γ of 10% (purple), 20% (red) and 30% (yellow). These curves have been plotted for $\eta = 0$ (plain lines), $\eta = 1$ (dashed lines) and $\eta = 5$ (dash-dotted lines).

Fig. 2.b). We then plot the evolution of $\widetilde{\text{CRB}}_{z_s} / \min_\Delta \widetilde{\text{CRB}}_{z_s}$ as a function of the noise parameter λ, and computed for $\widetilde{\Delta}$. The curves are plotted for several values of the relative error on δ ($\epsilon = 0\%, 10\%, 20\%, 30\%$) and for several values of η. Without any error on γ (blue curves), choosing Δ in the middle of the 20% interval leads to a very limited increase in CRB from optimal. With a large 30% error on γ (yellow curve), the increase in CRB with respect to optimal remains bounded by a factor of 1.4 (1.15 for an error of 20%, see red curve). When $\lambda \to 1$, *i.e.* as the contribution of the electronic noise β decreases, the CRB ratio tends to 1, which confirms the robustness of this approach to a certain mis-knowledge on γ.

In situations in which the a priori knowledge on γ is not precise enough, estimation performance may be far from optimal. To compensate this decrease of performance with respect to optimal, a possibility is to increase I_0. However, it results in increasing phototoxicity as well. In such situations, it can be interesting to use an iterative procedure. Rather than directly sending the whole photon budget I_0 on the tissue, we can perform a first acquisition with lower intensity, and with δ determined from Fig. 2.b using the user's prior on γ. This will then allow to perform further acquisitions with more precise priors on γ, and thus with values of $\widetilde{\text{CRB}}_{z_s}$ closer to optimal. Last but not least, such iterative approaches will also progressively provide a prior knowledge on the location z_s. This latter point has thus to be taken into account in the design of the scanning strategy, and will be analyzed in the next section.

4. OPTIMAL SAMPLING WITH PRIOR ON THE SURFACE LOCATION

In the previous section, we assumed no prior information on the position z_s. This led to a uniform distribution of the scanning points over the whole z-range. On practical terms however, one can sometimes have an approximate prior knowledge of z_s. This prior may come from previous estimation at neighboring points (x, y) or in the context of an iterative procedure (at given (x, y), an approximate estimation of the surface's location z_s precedes a more precise one). When z_s is approximately known, instead of scanning all the available z-space, we rather perform a few acquisitions around the approximate value of z_s.

In this section, we still assume that the K scanning points are regularly spaced by a constant δ. We study the influence of K and δ on the estimation performance, knowing that the total span of the scanning points no more needs to cover the full z-range $[z_{\min}, z_{\max}]$.

A. CRB expression

The scanning points z_k are positioned around the a priori value of z_s. We denote z_0 the center of the acquisition interval $[z_1; z_K]$, defined as $z_0 = (z_K + z_1)/2$. Our goal is to determine the optimal values of K, δ, and of the position z_0 of the interval $[z_1, z_K]$ with respect to the amount of prior knowledge we have on z_s.

In this case, the CRB of z_s can be written as

$$\text{CRB}_{z_s} = \frac{\gamma^2}{I_0^2 a^2} (\alpha I_0 b + \beta) \cdot \frac{K^2 [\widetilde{\mathbf{R}}^{-1}]_{1,1}}{\Delta^2} \tag{13}$$

where the coefficients $\widetilde{\Lambda}_{p,q}$ of the matrix $\widetilde{\mathbf{R}}$ take a different form than that of in the previous section:

$$\widetilde{\Lambda}_{p,q} = \sum_{k=1}^{K} \frac{(Z_k - Z_s)^p \, e^{-\frac{q(Z_k - Z_s)^2}{2}}}{\frac{\mu}{K} \left[1 + \eta e^{-\frac{(Z_k - Z_s)^2)}{2}} \right] + (1 - \mu)} \tag{14}$$

with

$$\mu = \frac{\alpha I_0 b}{\alpha I_0 b + \beta} \text{ and still } \eta = \frac{a}{b} \tag{15}$$

We have introduced a new parameter μ that replaces the parameter λ of section 3. Indeed, λ depends on the span $K\delta$ that is no more fixed to $l = z_{\max} - z_{\min}$. The parameter μ now represents the proportion of the signal-dependent noise with respect to the total amount of noise, considering the background signal only.

Thus, the quantity CRB_{z_s} depends on the scanning strategy (K, δ, and z_0) only through the quantity $K^2[\widetilde{\mathbf{R}}^{-1}]_{1,1}/\Delta^2$, which depends on the reduced parameters μ, η, Z_s and of course on $Z_1, Z_2, \ldots, Z_K$ (*i.e.* on $\Delta = \delta/\gamma$, K, and $Z_0 = z_0/\gamma$ the middle of $[Z_1; Z_K]$). In the following, the goal is to search for the optimal values of Δ, K and Z_0 that minimize this CRB.

The Fisher Information Matrix is non-invertible when $K < 3$ and in some situations when $K = 4$. We thus start our analysis with $K = 5$, as it corresponds to the simplest situation.

B. Analysis of the CRB when $K = 5$

Let us assume first that z_s is perfectly known. Figure 4.a shows the evolution of $\text{CRB}_{z_s} / \min_{\Delta, Z_0} \text{CRB}_{z_s}$ for $K = 5$ as a function of $Z_s - Z_0$ and of Δ. This normalized CRB depends on μ, η and on the acquisition parameters through the reduced variables $Z_s - Z_0 = (z_s - z_0)/\gamma$ and $\Delta = \delta/\gamma$. The black-contour plots correspond to $\mu = 0$ (electronic noise only) and to a signal-to-background ratio of $\eta \to 0$. The red-contour plots correspond to $\mu = 1$(pure signal-dependent noise) and $\eta \to \infty$. Whatever the values of η or μ, the minimum of CRB_{z_s} is reached for $Z_0 = Z_s$. Then, we have $\min_{\Delta, Z_0} \text{CRB}_{z_s} = \min_\Delta \text{CRB}_{z_s}|_{Z_0 = Z_s}$, and $\Delta_{opt} = \text{argmin}_\Delta \text{CRB}_{z_s}|_{Z_0 = Z_s}$.

Moreover, when $K = 5$, we can write from Eq. (13) and Eq. (14) the quantity $\min_\Delta \text{CRB}_{z_s}|_{Z_0 = Z_s}$ as a function of a single reduced coefficient $\mu\eta/(\mu\eta + 5 - 4\mu)$ instead of both μ and η. Figure 4.b shows the optimal spacing Δ_{opt} as a function

of this reduced parameter when $K = 5$ and $Z_0 = Z_s$ (black curve). We have also plotted the range of Δ values for which the increase in CRB remains within 20%, 50%, and 100% from the minimal CRB. It appears from these results that in situations where μ or η are not exactly known, setting for example $\Delta = \delta/\gamma = 0.7$ can be a robust solution, for which the increase in CRB always stays lower than 20%.

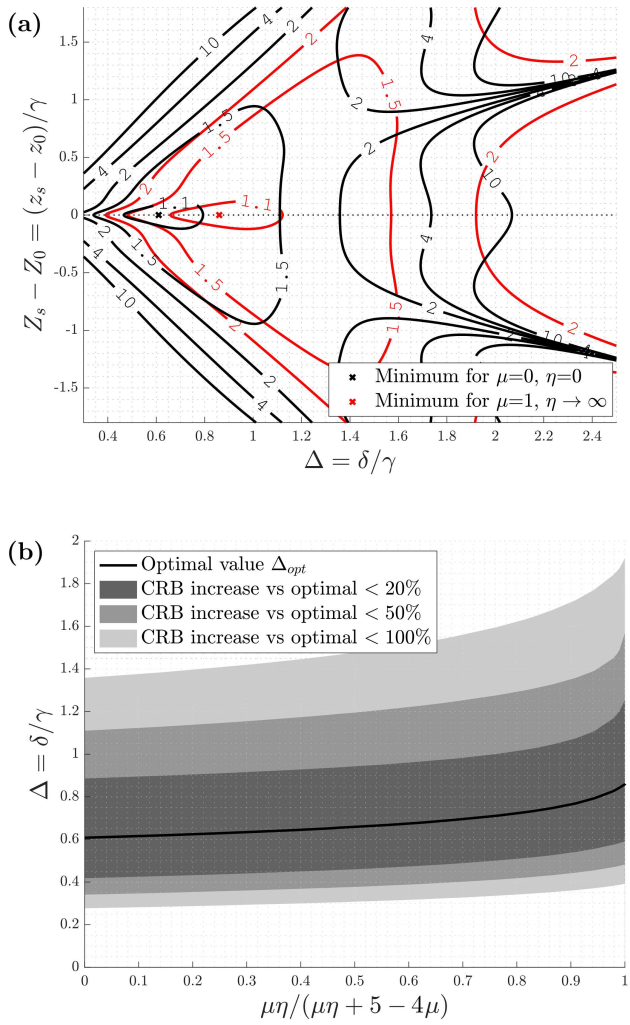

Fig. 4. Analysis when only $K = 5$ scanning points are used: (a) $\mathrm{CRB}_{z_s} / \min_{\Delta,Z_0} \mathrm{CRB}_{z_s}$ as a function of Δ and of the reduced variable $Z_s - Z_0$, with $Z_s = z_s/\gamma$ and $Z_0 = z_0/\gamma$, z_0 being the center of the sampling interval. The black-contour plots correspond to the case where $\mu = 0$ and $\eta \to 0$, while the red-contour plots correspond to the case where $\mu = 1$ and $\eta \to \infty$. The two crosses correspond to the locations where the CRB for both cases take their minimum. (b) When $z_0 = z_s$, evolution with respect to the reduced variable $\mu\eta/(\mu\eta + 5 - 4\mu)$ of the optimal value Δ_{opt} and of the Δ-ranges for which the CRB increase is lower than 20 %, 50 % and 100 % of its minimal value.

In Fig. 4.b, we set $Z_0 = Z_s$. It is of course not realistic, since z_s is the parameter to estimate. Since zs – and thus Zs – is only approximately known, we introduce $[Z_s^-, Z_s^+]$, which is the interval of possible Z_s-values. In order to take this interval into account in the optimization of the acquisition parameters, we still follow a minimax approach: we minimize the worst CRB value over all Z_s taking value in $[Z_s^-; Z_s^+]$. In other words, the optimization problem consists in finding the acquisition parameters Δ, K, Z_0) that minimize

$$\widetilde{\mathrm{CRB}}_{z_s} = \max_{Z_s \in [Z_s^-, Z_s^+]} K^2 [\widetilde{\mathbf{R}}^{-1}]_{1,1} / \Delta^2 \qquad \textbf{(16)}$$

As the CRB is symmetric with respect to $Z_0 - Z_s$ (see Fig. 4.a), Z_0 has to be set in the middle of $[Z_s^-, Z_s^+]$. In the following, we will thus fix Z_0 to $(Z_s^+ + Z_s^-)/2$.

In Fig. 5, we have plotted the evolution of $\widetilde{\mathrm{CRB}}_{z_s}$ as a function of the uncertainty $Z_s^+ - Z_s^-$, *i.e.* the length of $[Z_s^-, Z_s^+]$ (see blue curve for $K = 5$), when the signal-to-background ratio is set to $\eta = 2$ and the noise parameter to $\mu = 0.7$. This CRB has been computed for $\Delta = 0.7$, which is close to the optimal value Δ_{opt} when $Z_0 \approx Z_s$ and $K = 5$ (see Fig. 4.b). The signal-to-background ratio is set to $\eta = 2$, and the noise parameter is $\mu = 0.7$. It can be seen that the CRB increases quickly as the uncertainty $Z_s^+ - Z_s^-$ increases.

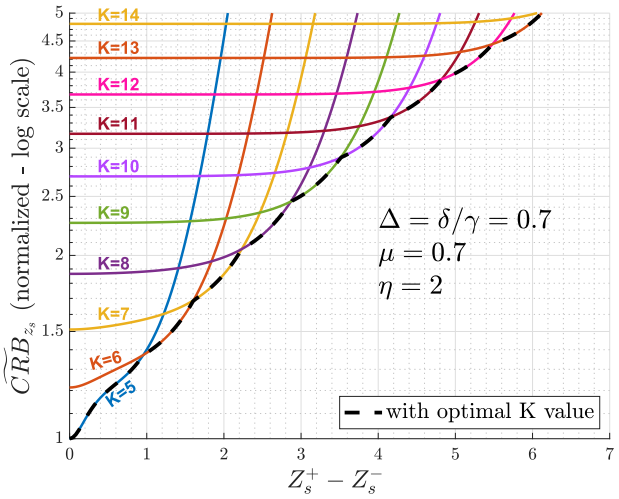

Fig. 5. Example, for $\mu = 0.7$ and $\eta = 2$, of the evolution of $\widetilde{\mathrm{CRB}}_{z_s}$ as a function of the uncertainty on Z_s (*i.e.* the value $Z_s^+ - Z_s^-$), when Δ is fixed to 0.7, and when K progressively increases from $K = 5$ to $K = 14$. This CRB has been normalized so that its minimum value (reached when $Z_s^+ - Z_s^- = 0$ and $K = 5$) is equal to 1. The value of $\widetilde{\mathrm{CRB}}_{z_s}$ computed with optimal K value has been super-imposed in black dashed line.

C. Analysis of the CRB in the general case

A solution to limit the increase in CRB is to add new scanning points while keeping Δ constant. Netherless, it results in the decrease in the intensity sent per each scanning point, as one operates at constant photon budget.

In Fig. 5, the evolution of $\widetilde{\mathrm{CRB}}_{z_s}$ obtained for $K = 6, 7, \ldots, 14$ has then been added to the curve obtained for $K = 5$. The lower envelop of all curves (dashed line) corresponds to $\min_K \widetilde{\mathrm{CRB}}_{z_s}$, *i.e.* to the values of $\widetilde{\mathrm{CRB}}_{z_s}$ for which the best K-value has been computed for each $Z_s^+ - Z_s^-$. We can see that changing the number K of scanning points allows to limit the increase in $\widetilde{\mathrm{CRB}}_{z_s}$ when the uncertainty on Z_s increases.

So far, in Fig. 5, we have fixed Δ to 0.7. We must address whether this choice on Δ is still relevant when the uncertainty on Z_s increases. We have thus plotted in Fig. 6.a

the evolution of $\min_K \widetilde{\mathrm{CRB}}_{z_s}$ (i.e. of $\widetilde{\mathrm{CRB}}_{z_s}$ with K set to its optimal value) for several Δ values, and still when $\mu = 0.7$ and $\eta = 2$. The lower envelope (red curve) provides an overall optimal CRB, for which the best K and Δ are selected for each uncertainty value $Z_s^+ - Z_s^-$. This envelope corresponds to $\min_{\Delta,K} \max_{Z_s \in [Z_s^-, Z_s^+]} \widetilde{\mathrm{CRB}}_{z_s}$ (with $\Delta = \delta/\gamma$ varying between 0.01 and 2 with a step of 0.01 for this curve). It appears that the optimal couple (K, Δ) changes rapidly with the uncertainty $Z_s^+ - Z_s^-$. Thus, one cannot rely on a single Δ to be optimal in a wide range of Z_s uncertainty. One rigorous but fastidious way to optimize the estimation would be to provide the best couple of parameters Δ and K for each $Z_s^+ - Z_s^-$, and of course for several values of the parameters μ and η.

To further gain insight in the choice of Δ, we emphasize the case $\Delta = 0.7$ (in blue on Fig. 5.b), which has been shown to be quasi-optimal when $Z_0 \approx Z_s$ and $K = 5$, whatever the values of μ and η (see Fig. 4.b). As expected, the curve appears near optimal at low values of $Z_s^+ - Z_s^-$, but increases much faster than optimal for $Z_s^+ - Z_s^- > 0.3$. As $Z_s^+ - Z_s^-$ becomes larger, the number of scanning points has to be increased, and we gradually approach the case of estimating z_s without prior, dealt in the previous section. A large number of scanning points at constant photon budget implies fewer photons per points. The noise variance is then increasingly dominated by the variance β of the electronic noise. Therefore, when $Z_s^+ - Z_s^- \gg 1$, the optimization becomes equivalent to the case without prior and $\lambda \to 0$. For this case, the optimal choice was around $\Delta = 1.3$ (see previous section). The curve for which $\Delta = 1.3$ has thus been underlined in Fig. 6.a (in green).

These two extreme settings $\Delta = 0.7$ and $\Delta = 1.3$ lead to performance close to those obtained with optimal Δ and K settings (red curve in Fig. 6.a). In Fig. 6.b, we have plotted the ratio of $\min_K \widetilde{\mathrm{CRB}}_{z_s}$ (*i.e.* $\widetilde{\mathrm{CRB}}_{z_s}$ with optimized K value) for $\Delta = 0.7$ or $\Delta = 1.3$, over $\min_{\Delta,K} \widetilde{\mathrm{CRB}}_{z_s}$ (*i.e.* . $\widetilde{\mathrm{CRB}}_{z_s}$ with both optimal Δ and K settings), still when $\mu = 0.7$ and $\eta = 2$. It appears that if we choose $\Delta = 0.7$ when $Z_s^+ - Z_s^- \lesssim 2$ and $\Delta = 1.3$ otherwise, the cost with respect to the optimal $\min_{\Delta,K} \widetilde{\mathrm{CRB}}_{z_s}$ value remains lower than a factor 1.21 *i.e.* the increase in CRB from optimal will stay under 21%.

D. Simplified two-spacing strategy

Following this analysis, we propose an alternative strategy to the systematic determination of the optimal parameters Δ and K. This simpler approach is to only consider the setting $\Delta = 0.7$ for small values of the uncertainty $Z_s^+ - Z_s^-$, and $\Delta = 1.3$ otherwise. There remains now to determine the value $Z_s^+ - Z_s^-$ where the transition between these two solutions occurs. We have seen that this transition happened for $Z_s^+ - Z_s^+ \simeq 2$ when $\mu = 0.7$ and $\eta = 2$ (see Fig. 6.b). In Fig. 7.a, we have plotted this transition with respect to μ, and for both $\eta = 5$ and $\eta \to 0$. For values of $Z_s^+ - Z_s^-$ below this transition, the scanning has to be done with $\Delta = 0.7$, while it has to be performed with $\Delta = 1.3$ above this transition. Furthermore, the optimal values of K corresponding to each situation have also been reported on this graph.

Considering this simplified strategy, a question arises: how much do we lose by using this simplified strategy instead of using the strategy with optimal Δ and K? To address this point, we show in Fig. 7.b (blue curves) the ratio of $\widetilde{\mathrm{CRB}}_{z_s}$ obtained with the simplified strategy and of $\min_{\Delta,K} \widetilde{\mathrm{CRB}}_{z_s}$ obtained with optimal Δ and K settings. This ratio depends on η, μ and $Z_s^+ - Z_s^-$. For the sake of simplicity, we have plotted the worst

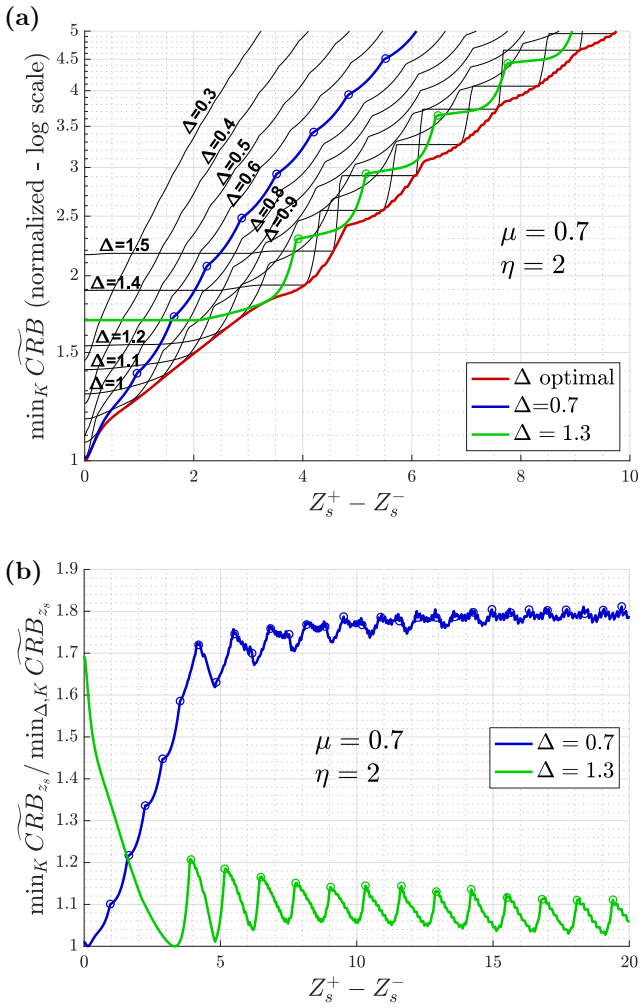

Fig. 6. Example for $\mu = 0.7$ and $\eta = 2$: (a) evolution of $\widetilde{\mathrm{CRB}}_{z_s}$ as a function of the uncertainty on Z_s, for different values of Δ and with selecting for each uncertainty value the optimal number K of scanning points. This CRB has been normalized so that its minimum value (reached when $Z_s^+ - Z_s^- = 0$ and $K = 5$) is equal to 1. The blue line corresponds to $\Delta = 0.7$ and the green one to $\Delta = 1.3$. The circle points indicate where the optimal values of K increase by 1. The red line corresponds to the optimal setting of both K and Δ among all possible values (with Δ sampled with a step of 0.01). (b) Evolution of $\min_K \widetilde{\mathrm{CRB}}_{z_s}$ divided by the optimal CRB value $\min_{\Delta,K} \widetilde{\mathrm{CRB}}_{z_s}$ (optimized both on K and Δ), as a function of the uncertainty $Z_c^+ - Z_c^-$ on Z_s, when Δ is fixed to 0.7 (blue curve) and to 1.3 (green curve).

CRB ratio *i.e.* the highest ratio over all values of $Z_s^+ - Z_s^-$ as a function of the noise parameter μ, and for several η values. It appears that the increase in CRB is very limited. The maximal increase in CRB is obtained for $\mu = 0$, with a ratio of 1.32 (see blue curve in Fig. 7.b). Note that, to keep performance level close to optimal, this can be compensated by increasing the photon budget I_0 by 32%.

Finally, we investigate the robustness of this simplified strategy to an error on γ. In Fig. 7.b, we have added the ratio when assuming an error ϵ on γ of 10% (violet curves), 20% (red curves) and 30% (yellow curves). It can be seen that the conse-

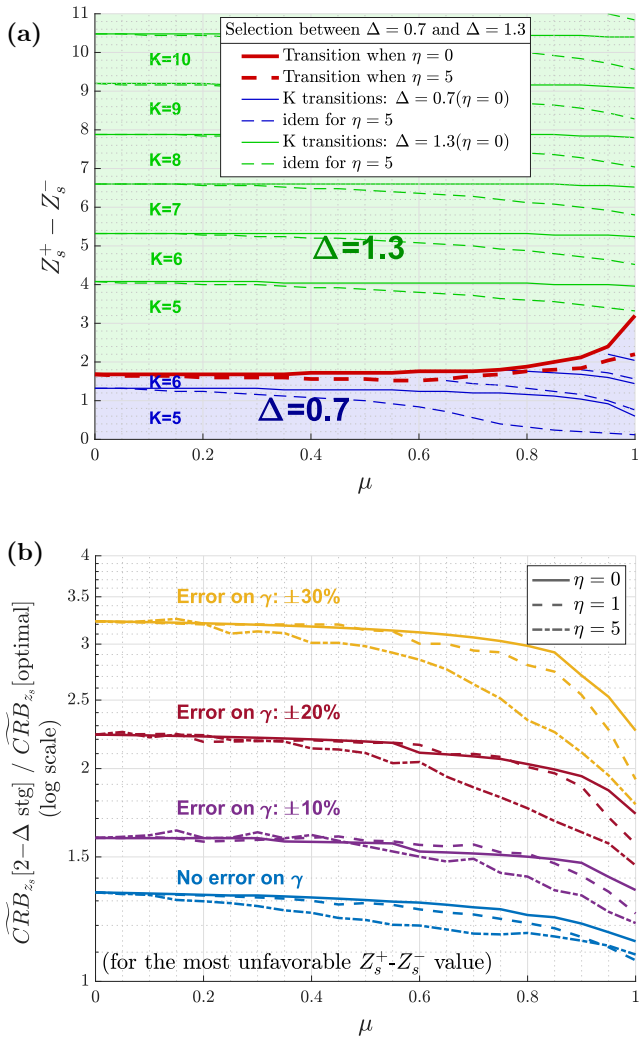

Fig. 7. (a) Selection between $\Delta = 0.7$ (blue zone) and $\Delta = 1.3$ (green zone) as a function of μ and of the uncertainty on Z_s (i.e. $Z_s^+ - Z_s^-$). The frontier between these two situations has been plotted with a red line. The optimal choice of K has also been reported on this graph (with frontiers marked with green or blue lines). These curves have been plotted for $\eta = 0$ (plain lines) and $\eta = 5$ (dashed lines). (b) Robustness to the knowledge of γ. Evolution, as a function of μ, of the ratio of $\widetilde{\mathrm{CRB}}_{z_s}$ obtained using the approach proposed in (a) to that of obtained with optimal Δ and K values. The ratio is computed for the most unfavorable uncertainty $Z_s^+ - Z_s^-$, *i.e.* the uncertainty that leads to the highest CRB ratio. This ratio has been plotted first in the ideal case where γ is perfectly known (in blue), and then in the case of an error on γ of 10% (purple), 20% (red) and 30% (yellow). These curves have been plotted for $\eta = 0$ (plain lines), $\eta = 1$ (dashed lines) and $\eta = 5$ (dash-dotted lines).

quences of a mis-knowledge of γ in the case of a prior are more important than that of without prior (cf. previous section and Fig. 3). For example, an error on γ of 30% leads this time to an increase in the CRB by a factor of 3.2, which is to compare with an increase by a factor of 1.4 when having no prior on z_s. This difference comes from the fact that this time, an error on γ will result in an error on the transition point between the $\Delta = 1.3$ and $\Delta = 0.7$ domains, but also on the determination of K. Nevertheless, it should be pointed out that as soon as a prior on z_s is available, a quite good prior on γ can be expected thus limiting the error on γ and the increase in CRB.

5. CONCLUSION

In this paper, we have proposed a CRB-based approach to optimize the scanning strategy along z-axis, given a fixed photon budget, when the goal is to determine the location z_s of a labeled biological surface. Here, the fluorescent signal was modeled as a Gaussian shape centered on z_s and corrupted by additive signal-dependent noise. The problem of estimating z_s at fixed photon budget, depends on numerous parameters: parameters related to the acquisition process (noise, photon budget, scanning strategy) and parameters related to the model, including z_s itself. It also depends on the amount of prior knowledge we have on z_s. We have shown that in case of regular sampling, by introducing a controlled loss in the estimation precision, we can design general scanning strategies that only depend on a few reduced parameters.

Without prior knowledge on z_s, the strategy is to scan regularly the full z-space. In this situation, the optimal spacing δ between two consecutive scanning points only depends on γ, which is related to the width of the tissue modeled by the Gaussian shape, on the signal-to-background ration η, and on the noise parameter λ, which account for the proportion of pure signal-dependent noise with respect to the total amount of noise in the acquisition process. Moreover, when the spacing is set to 1.3γ, the increase in CRB from its optimal value will always stay under 20 %, whatever the value of the parameters λ and η. When prior knowledge on z_s is available, a quasi optimal strategy has been proposed in which two situations may occur. If the interval of a priori z_s-values is thinner than approximately 2γ, the scanning point should be separated by 0.7γ. Otherwise, they should once again be separated by 1.3γ.

As a perspective, theoretical questions related to this work remain. In particular, we have only addressed the case of regular sampling strategies with same intensity sent on all the scanned points. Although non-regular sampling strategies should intuitively lead to a lower CRB, notably in the case of an a priori knowledge on the location of the Gaussian, determining the optimal sampling over all possible strategies is far from trivial. Moreover, this will then require a fine study of the trade-off between the CRB decrease that can be obtained using an irregular sampling, versus the increase in complexity, not only in term of experimental ease of use but also in term of robustness to physical parameter variations.

Future work will also need to implement and test experimentally the proposed scanning strategy on real biological tissues. The main advantage of this strategy is that it can be easily implemented in 3D-scanning microscopes with targeted illumination such as proposed in [12, 24, 25]. Moreover, an adaptive scanning scheme can be derived from the proposed approach. In this case, the estimation of z_s can be converted to a prior for the next round of estimation, while the interval of a priori z_s-values $[z_s^-, z_s^+]$ can directly be linked to the CRB of z_s obtained from Eq. 4 e.g. as $z_s^+ - z_s^- \approx 3\sqrt{\mathrm{CRB}_{z_s}}$ for efficient estimators using a typical 3-σ confidence interval. Next step is then to recover the surface that best fits the set of z_s estimates $\widehat{z}_i$ obtained from the z-scans performed at different (x_i, y_i) coordinates ($i = 1, 2, 3, \ldots$). Furthermore, depending on the a priori on the surface model – particularly its smoothness – the optimal choice of the set of coordinates (x_i, y_i) that achieves

the best trade-offs between the precision of surface estimation and photon budget is an interesting perspective of this work. Eventually, it is worth noting that this paper focused on the estimation precision of z_s only, even though the whole parameters of the model – including the width of the tissue – were estimated simultaneously. It would be interesting to draw scanning schemes that consider jointly the estimation precision of the position and of the width of the biological surface.

A. FISHER INFORMATION MATRIX FOR Z_S ESTIMATION

Let $\boldsymbol{\theta} = (z_s, \gamma, a, b)^T$ the model parameter vector to estimate. The log-likelihood of the acquired sample $\chi = \{s(z_1), \dots, s(z_K)\}$ is equal to

$$\ell(\chi|\boldsymbol{\theta}) = -\frac{1}{2}\sum_{k=1}^{K} \ln\{2\pi[\alpha r(z_k)+\beta]\} - \frac{1}{2}\sum_{k=1}^{K}\frac{[s(z_k)-r(z_k)]^2}{\alpha r(z_k)+\beta}$$

The Fisher information matrix $\mathbf{J}$ is the 4×4 matrix so that, for $n, m \in [\![1,4]\!]$,

$$\begin{aligned}[\mathbf{J}]_{n,m} &= -\left\langle \frac{\partial^2 \ell(\chi|\boldsymbol{\theta})}{\partial\theta_n \partial\theta_m}\right\rangle \\ &= \sum_{k=1}^{K}\frac{\partial r(z_k)}{\partial\theta_n}\frac{\partial r(z_k)}{\partial\theta_m}\frac{1}{\alpha r(z_k)+\beta}\left[1+\frac{\alpha^2}{2\alpha r(z_k)+2\beta}\right]\end{aligned}$$

with θ_n denoting the n^{th} component of vector $\boldsymbol{\theta}$. As in [15], as soon as the number of counts on the sensor is not too small, the Fisher information matrix $\mathbf{J}$ becomes

$$[\mathbf{J}]_{n,m} = \sum_{k=1}^{K}\frac{\partial r(z_k)}{\partial\theta_n}\cdot\frac{\partial r(z_k)}{\partial\theta_m}\cdot\frac{1}{\alpha r(z_k)+\beta} \tag{17}$$

with

$$\begin{aligned}\frac{\partial r(z_k)}{\partial z_s} &= \frac{aI_0}{K}\frac{z_k-z_s}{\gamma^2}\exp\left[-\frac{(z_k-z_s)^2}{2\gamma^2}\right] \\ \frac{\partial r(z_k)}{\partial \gamma} &= \frac{aI_0}{K}\frac{(z_k-z_s)^2}{\gamma^3}\exp\left[-\frac{(z_k-z_s)^2}{2\gamma^2}\right] \\ \frac{\partial r(z_k)}{\partial a} &= \frac{I_0}{K}\exp\left[-\frac{(z_k-z_s)^2}{2\gamma^2}\right] \\ \frac{\partial r(z_k)}{\partial b} &= \frac{I_0}{K}\end{aligned} \tag{18}$$

Following Eq. (17) and Eq. (18), $\mathbf{J}$ can be written as

$$\mathbf{J} = \frac{I_0^2}{K^2}\begin{bmatrix} \frac{a^2}{\gamma^2}\Lambda_{2,2} & \frac{a^2}{\gamma^2}\Lambda_{3,2} & \frac{a}{\gamma}\Lambda_{1,2} & \frac{a}{\gamma}\Lambda_{1,1} \\ \frac{a^2}{\gamma^2}\Lambda_{3,2} & \frac{a^2}{\gamma^2}\Lambda_{4,2} & \frac{a}{\gamma}\Lambda_{2,2} & \frac{a}{\gamma}\Lambda_{2,1} \\ \frac{a}{\gamma}\Lambda_{1,2} & \frac{a}{\gamma}\Lambda_{2,2} & \Lambda_{0,2} & \Lambda_{0,1} \\ \frac{a}{\gamma}\Lambda_{1,1} & \frac{a}{\gamma}\Lambda_{2,1} & \Lambda_{0,1} & \Lambda_{0,0}\end{bmatrix} \tag{19}$$

with $\Lambda_{p,q}$ expressions given in Eq. (6). The CRB on z_s is thus

$$\text{CRB}_{z_s} = [\mathbf{J}^{-1}]_{1,1} = \frac{[\text{adj}(\mathbf{J})]_{1,1}}{\det\mathbf{J}} \tag{20}$$

where $\text{adj}(\mathbf{J})$ denotes the adjugate matrix of $\mathbf{J}$, and $\det(\mathbf{J})$ denotes the determinant of $\mathbf{J}$. The cofactor $[\text{adj}(\mathbf{J})]_{1,1}$ is the determinant of the submatrix of $\mathbf{J}$ formed by removing the first row and first column. By developing the expression of the determinants of both matrices, and by using the expression of $\mathbf{R}$ given in Eq. (5), we obtain that $\det(\mathbf{J}) = (\frac{I_0^2 a}{K^2\gamma})^4\det(\mathbf{R})$ and $[\text{adj}(\mathbf{J})]_{1,1} = (\frac{I_0}{K})^6(\frac{a}{\gamma})^2[\text{adj}(\mathbf{R})]_{1,1}$, which lead to Eq. (4).

Funding. Agence Nationale de la Recherche (ANR-18-CE13-028, ANR-17-CE30-0007) ; Excellence Initiative of Aix-Marseille University - A*Midex (capostromex), a French Investissements d'Avenir programme; The project leading to this publication has received funding from the "Investissements d'Avenir" French Government program managed by the French National Research Agency (ANR-16-CONV-0001, ANR-21-ESRE-0002) and from Excellence Initiative of Aix-Marseille University - A*MIDEX.

Acknowledgments. We thank Philippe Réfrégier, Sophie Brasselet, Hervé Rigneault and Vincent Bertrand for fruitful discussions on the project.

Disclosures. The authors declare no conflicts of interest.

Data availability. Data underlying the results presented in this paper are not publicly available at this time but may be obtained from the authors upon reasonable request.

REFERENCES

1. P. M. Carlton, J. Boulanger, C. Kervrann, J.-B. Sibarita, J. Salamero, S. Gordon-Messer, D. Bressan, J. E. Haber, S. Haase, L. Shao, L. Winoto, A. Matsuda, P. Kner, S. Uzawa, M. Gustafsson, Z. Kam, D. A. Agard, and J. W. Sedat, "Fast live simultaneous multiwavelength four-dimensional optical microscopy," Proc. Natl. Acad. Sci. **107**, 16016–16022 (2010).
2. C. Boudreau, T.-L. E. Wee, Y.-R. S. Duh, M. P. Couto, K. H. Ardakani, and C. M. Brown, "Excitation light dose engineering to reduce photobleaching and photo-toxicity," Sci. Reports **6**, 30892 (2016).
3. R. Hoebe, C. Van Oven, T. W. Gadella, P. Dhonukshe, C. Van Noorden, and E. Manders, "Controlled light-exposure microscopy reduces photobleaching and phototoxicity in fluorescence live-cell imaging," Nat. biotechnology **25**, 249–253 (2007).
4. K. K. Chu, D. Lim, and J. Mertz, "Enhanced weak-signal sensitivity in two-photon microscopy by adaptive illumination," Opt. letters **32**, 2846–2848 (2007).
5. T. Staudt, A. Engler, E. Rittweger, B. Harke, J. Engelhardt, and S. W. Hell, "Far-field optical nanoscopy with reduced number of state transition cycles," Opt. express **19**, 5644–5657 (2011).
6. J. Dreier, M. Castello, G. Coceano, R. Cáceres, J. Plastino, G. Vicidomini, and I. Testa, "Smart scanning for low-illumination and fast RESOLFT nanoscopy in vivo," Nat. communications **10**, 1–11 (2019).
7. B. Vinçon, C. Geisler, and A. Egner, "Pixel hopping enables fast sted nanoscopy at low light dose," Opt. express **28**, 4516–4528 (2020).
8. M. Weigert, U. Schmidt, T. Boothe, A. Müller, A. Dibrov, A. Jain, B. Wilhelm, D. Schmidt, C. Broaddus, S. Culley, M. Rocha-Martins, F. Segovia-Miranda, C. Norden, R. Henriques, M. Zerial, M. Solimena, J. Rink, P. Tomancak, L. Royer, F. Jug, and E. W. Myers, "Content-aware image restoration: pushing the limits of fluorescence microscopy," Nat. Methods **15**, 1090–1097 (2018).
9. L. Jin, B. Liu, F. Zhao, S. Hahn, B. Dong, R. Song, T. C. Elston, Y. Xu, and K. M. Hahn, "Deep learning enables structured illumination microscopy with low light levels and enhanced speed," Nat. Commun. **11**, 1934 (2020).
10. F. Strobl, A. Schmitz, and E. H. Stelzer, "Improving your four-dimensional image: traveling through a decade of light-sheet-based fluorescence microscopy research," Nat. protocols **12**, 1103 (2017).
11. M. Woringer, X. Darzacq, C. Zimmer, and M. Mir, "Faster and less phototoxic 3d fluorescence microscopy using a versatile compressed sensing scheme," Opt. Express **25**, 13668–13683 (2017).
12. F. Abouakil, H. Meng, M.-A. Burcklen, H. Rigneault, F. Galland, and L. Le Goff, "An adaptive microscope for the imaging of biological surfaces," Light: Science and Applications **10**, 210 (2021).
13. H. Meng, D. Nuzhdin, M. Sison, F. Galland, and L. LeGoff, "Adaptive scans allow targeted cell-ablations on curved cell sheets," BioRxiv (2022).

14. P. Garthwaite, I. Joliffe, and B. Jones, Statistical Inference (2002).
15. M. Boffety, F. Galland, and A.-G. Allais, "Influence of polarization filtering on image registration precision in underwater conditions," Opt. Lett. **37**, 3273–3275 (2012).
16. P. Réfrégier, C. Scotté, H. B. de Aguiar, H. Rigneault, and F. Galland, "Precision of proportion estimation with binary compressed raman spectrum," J. Opt. Soc. Am. A **35**, 125–134 (2018).
17. O. Lévêque, C. Kulcsár, A. Lee, H. Sauer, A. Aleksanyan, P. Bon, L. Cognet, and F. Goudail, "Co-designed annular binary phase masks for depth-of-field extension in single-molecule localization microscopy," Opt. Express **28**, 32426–32446 (2020).
18. J. V. Beira and R. Paro, "The legacy of drosophila imaginal discs," Chromosoma **125**, 573–592 (2016).
19. J. Huang, W. Zhou, W. Dong, A. M. Watson, and Y. Hong, "Directed, efficient, and versatile modifications of the drosophila genome by genomic engineering," Proc. Natl. Acad. Sci. **106**, 8284–8289 (2009).
20. J. Chao, E. S. Ward, and R. J. Ober, "Fisher information matrix for branching processes with application to electron-multiplying charge-coupled devices," Multidimens. Syst. Signal Process. **23**, 349–379 (2012).
21. S. Mailfert, J. Touvier, L. Benyoussef, R. Fabre, A. Rabaoui, M.-C. Blache, Y. Hamon, S. Brustlein, S. Monneret, D. Marguet, and N. Bertaux, "A theoretical high-density nanoscopy study leads to the design of unloc, a parameter-free algorithm," Biophys. J. **115**, 565–576 (2018).
22. B. Mandracchia, X. Hua, C. Guo, J. Son, T. M. Urner, and S. Jia, "Fast and accurate scmos noise correction for fluorescence microscopy," Nat. Commun. **11**, 94 (2020).
23. N. Hagen, M. Kupinski, and E. L. Dereniak, "Gaussian profile estimation in one dimension," Appl. Opt. **46**, 5374–5383 (2007).
24. N. Chakrova, A. S. Canton, C. Danelon, S. Stallinga, and B. Rieger, "Adaptive illumination reduces photobleaching in structured illumination microscopy," Biomed. Opt. Express **7**, 4263–4274 (2016).
25. H. Pinkard, H. Baghdassarian, A. Mujal, E. Roberts, K. H. Hu, D. H. Friedman, I. Malenica, T. Shagam, A. Fries, K. Corbin, M. F. Krummel, and L. Waller, "Learned adaptive multiphoton illumination microscopy for large-scale immune response imaging," Nat. Commun. **12**, 1916 (2021).